The Journal of Chemical Physics

Time resolved mechanism of the isotope selectivity in the ultrafast light induced dissociation in N_2

Cite as: J. Chem. Phys. **151**, 114308 (2019); https://doi.org/10.1063/1.5118990
Submitted: 09 July 2019 . Accepted: 27 August 2019 . Published Online: 19 September 2019

Ksenia G. Komarova, Francoise Remacle, and R. D. Levine

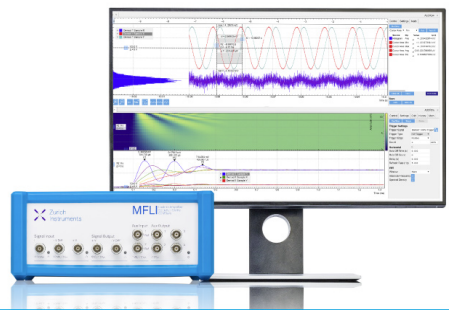

AIP Publishing

The Journal of Chemical Physics ARTICLE scitation.org/journal/jcp

Time resolved mechanism of the isotope selectivity in the ultrafast light induced dissociation in N_2

Cite as: J. Chem. Phys. 151, 114308 (2019); doi: 10.1063/1.5118990
Submitted: 9 July 2019 • Accepted: 27 August 2019 •
Published Online: 19 September 2019

Ksenia G. Komarova,[1,a] Francoise Remacle,[1,2] and R. D. Levine[1,3,4]

AFFILIATIONS

[1]The Fritz Haber Center for Molecular Dynamics and Institute of Chemistry, The Hebrew University of Jerusalem, Jerusalem 91904, Israel
[2]Theoretical Physical Chemistry, UR MolSys B6c, University of Liège, B4000 Liège, Belgium
[3]Department of Molecular and Medical Pharmacology, David Geffen School of Medicine, Los Angeles, California 90095, USA
[4]Department of Chemistry and Biochemistry, University of California, Los Angeles, California 90095, USA

Note: This paper is part of the JCP Special Collection on Ultrafast Spectroscopy and Diffraction from XUV to X-ray.
[a]**Electronic mail:** kgvladi@fh.huji.ac.il

ABSTRACT

The time evolution of a vacuum ultraviolet excited N_2 molecule is followed all the way from an ultrafast excitation to dissociation by a quantum mechanical simulation. The primary aim is to discern the role of the excitation by a pulse short compared to the vibrational period, to discern the different coupling mechanisms between different electronic states, nonadiabatic, spin orbit, and to analyze the origin of any isotopic effect. We compare the picture in the time and energy domains. The initial ultrafast excitation pumps the molecule to a coherent electronic wave packet to which several singlet bound electronic states contribute. The total nonstationary wave function is given as a coherent sum of nuclear wave packets on each electronic state times the stationary electronic wave function. When the wave packets on different electronic states overlap, they are coupled in a mass-dependent manner whether one uses an adiabatic or a diabatic electronic basis. A weak spin-orbit coupling acts as a bottleneck between the bound singlet part of phase space and the triplet manifold of states in which dissociation takes place. To describe the spin-orbit perturbation that is ongoing in time, an energy-resolved eigenstate representation appears to be more intuitive. In the eigenstate basis, the singlet-to-triplet population transfer is large only between those vibronic eigenstates that are quasiresonant in energy. The states in resonance are different for different excitation energy ranges. The resonances are mass dependent, which explains the control of the isotope effect through the profile of the pulse.

I. INTRODUCTION

Ultrafast light pulse induced dynamics in molecules enables a time-domain picture of photochemical reaction dynamics. For pulses shorter than periods of nuclear motions, molecules pumped to excited states have localized origin in time and space of the nuclear coordinates.[1,2] Thereby, "femtochemistry"[2] allows monitoring the chemical change as reflected in structural rearrangement in real time. Atto- or few femtosecond pulses resolve even deeper: one can pump the electrons to a nonequilibrated state and follow electron dynamics on a time scale before they are adjusted to the instantaneous position of the nuclei.[3–8] Ultrafast pumping allows probing the wave character of the nuclear dynamics,[9] and with attosecond pumping, one begins to probe the wave character of the electron dynamics.[10,11] Coherent excitation of the ground state creates a wave packet of electronic states to which several electronic states coherently contribute. In polyatomic molecules, there is a whole forest of accessible electronic states, and even in diatomics of atmospheric interest, O_2, N_2, CO, etc., several excited states can be populated. In the case of N_2, there is strong mixing between the

singlet states and a weak singlet-triplet coupling that acts to separate the bound singlet states from the triplets, some of which are dissociative. The populations of the initially excited electronic states are determined by their transition dipole moment from the ground state, by the Franck-Condon factors, and by the pulse parameters such as its width in energy, its polarization,[12] and the carrier-envelope phase (CEP) between the envelope of the pulse and the carrier wave.[13,14]

In the energy domain picture, the ultrafast excitation produces an N_2 molecule in a bound (the singlet) part of its phase space in a broad energy range. In the case of coupling between the excited electronic states, there will be dynamical mixing between them. This is a picture with an analogy to the Lindeman mechanism[15] for vibrational dissociation of collision excited polyatomics. Inherent in the Lindeman mechanism is the mixing of the bound vibrational states sometimes called the sampling of phase space. Here, after the laser field is over, we have a sampling of the electronic phase space in the singlet manifold. In the long pulse limit, there will not be an exploration of the phase space after the excitation. A feature not typically discussed in the Lindeman mechanism is that past the barrier, en route to dissociation induced by a fast pulse, there is still dynamical interaction between the bound and repulsive triplet states. Diagonalizing the states in the triplet manifold can be viewed as an electronic analog of the adiabatic channel model of Quack and Troe.[16] The remaining, not weak, nonadiabatic coupling (NAC) between bound and dissociative triplet states means that the atoms can begin to separate but are then returned as in the healing concept of Hall and Levine.[17]

The nuclear motion of the ultrafast pumped wave packet can be viewed as a molecular analog to the several-slit experiment in that the molecule is evolving coherently in several electronic potentials. The nuclear wave packets pumped in the Franck-Condon region to different electronic potentials have initially similar localization in nuclear coordinates and similar phases. As the dynamics unfolds, each of the wave packets will trace different paths, according to the bonding nature of the electronic states involved. This will result in the time-dependent phase shift between the two wave packets and therefore interference patterns in their overlap. Recently, we described[18] such an effect for the case of the ultrafast field-induced dynamics in valence and Rydberg singlet states of N_2. In the case of N_2, strong nonadiabatic coupling between these states is localized in the Franck-Condon region. When the wave packets return to the coupling region, the effective rate of transfer between them depends on their overlap and therefore is sensitive to the relative phases accumulated along their unique paths. An essentially quantum feature of the nuclei—the time-dependent phase of the wave packet—can be probed via indirect measures of the rate or even direction of the population transfer between different electronic states. We showed that an effective tool of chemical kinetics—the measurement of the isotope effect—can be used as a probe for the interference patterns already at early time of the dynamics.

In this paper, we discuss an excitation of N_2 by an ultrafast vacuum ultraviolet (VUV) pulse and follow the dynamics of the system all the way to dissociation. The high resolution spectroscopy of isotopomers of N_2 has been very thoroughly studied.[19–23] Rotationally resolved spectra allowed determination of the linewidths including those for the heavier isotopomer.[22,23] Several models[24–31] were developed to reproduce the database of the experimental measurements on the positions, widths, and lifetimes which correspond to particular vibronic levels. The most relevant for the present work are results of fitting of the singlet state diabatic potentials and their coupling done by Spelsberg and Meyer[24] on the basis of high-level *ab initio* quantum chemistry calculations. Based on these data for the singlet states, a predissociation model of the lowest energy $^1\Pi_u$ levels, including spin-orbit (SO) coupling between the singlet and triplet states of the same symmetry, was developed by Lewis and Lefebvre-Brion *et al.*[26] The very weak singlet triplet coupling is stronger between the bound singlet valence excited state and a bound triplet state. The spin orbit coupling is four times weaker to the other low energy repulsive triplet state. These two triplet states are coupled among themselves by a relatively strong coupling. References 24–26 provide details on the experimental spectroscopic database used to build the predissociation model. Model studies were also used to discuss isotopic selectivity in the photo dissociation.[23]

Depending on the excitation energy, there are at least three dissociation channels that can contribute. Recent experiments on the branching ratios for different channels by Jackson *et al.*[29] show that at the low energy region of the absorption spectrum, 100 000–112 000 cm^{-1}, there is only one pathway that is energetically open and we will discuss it in Sec. II in more detail. However, even for this low energy region with one open channel, strong isotope effect in the dissociation yield was observed by Thiemens *et al.*[32] and was shown to be considerably excitation energy-dependent.

The picture that emerged from the highly energy resolved studies is that of a slow electronic predissociation from a bound singlet state. The width in energy of the predissociating states is low enough that the individual rotational states are resolved. In this paper, we trace the time history of the excited wave packet, which is a superposition of several electronic energy resolved states each with its own weight and phase. The singlet states of N_2, optically accessible from the ground state by a one photon transition, are all bound in the energy range of interest. We here focus on the long-term process of intersystem crossing—how the initially pumped coherent wave packet is probed by the weak coupling to the triplets. In particular, we want to follow the fate of the time-dependent isotope effect discussed above for the population dynamics of the singlet states.[18] We will show that a resonance like condition arises through the weak but long acting singlet-triplet coupling. This has two implications. One is that because the coupling is weak, the dynamics of the singlet states is hardly perturbed and their dynamical mixing persists undiminished. A second and experimentally relevant point is that the resonance condition in the singlet-triplet coupling modulates the long term isotope effect in the yield of dissociation. Thereby even the sign of the effect can be controlled by using different energy profiles of the excitation pulses.

The paper is organized as follows. In Sec. II, we discuss the correspondence between the adiabatic and diabatic representations of the coupled states in N_2. We pay special attention to the dependence of the coupling between states on the internuclear distance R. The relevant electronic states for the photodissociation at the energy range of interest are used to build a model set of potentials and analyze the intersystem crossing process for the initially excited coherent wave packet in more detail. In Sec. III, the details of the ultrafast field induced quantum dynamics both in singlet and

triplet manifolds are provided. We discuss, in detail, excitation by two ultrafast pulses with central frequencies centered at a low and a somewhat higher energy region. Next, Sec. IV presents the computational results for the isotope effect on dissociation yields for $^{14}N_2$, $^{14}N^{15}N$, and $^{15}N_2$.

II. ADIABATIC AND DIABATIC STATES OF N_2

A. Details of the quantum chemistry computations

Adiabatic singlet and triplet Π_u states were described using a multiconfigurational self-consistent field (MCSCF) approach[33–35] followed by multireference configuration interaction[36,37] calculations using MOLPRO.[38] Potential energy curves, transition dipole moments, nonadiabatic, and spin-orbit couplings were computed within the same set of active orbitals for the singlet and triplet manifold of states. An active space of 16 orbitals ($3\sigma_u$, $3\sigma_g$, $4\pi_u$, $4\pi_g$, and $2\delta_g$) for 10 valence electrons was optimized following the stepwise procedure suggested by Spelsberg and Meyer[24] to achieve good accuracy for the optically active states. In the energy range of interest, the nonadiabatic coupling (NAC) terms within both the singlet and triplet manifolds are large; therefore, the state averaging method[33,36] of MCSCF was used to reach a balanced description for all the states of interest. 5 singlet and 10 triplet states were included in the averaging procedure. To achieve convergence at a reasonable computational cost, potentials, transition dipoles, and nonadiabatic couplings were computed separately for the states of different multiplicity. Only spin-orbit coupling terms were calculated with averaging over the states of both multiplicities. The correspondence between the two runs was found on the basis of similar population of configuration classes for each electronic state. All calculations employed a doubly augmented cc-pVQZ[39,40] basis set with additional bond-centered *s* and *p* diffuse functions[41] for a proper description of Rydberg and valence states. For singlet potentials and composition of states, good correspondence was found between our results and those of Spelsberg and Meyer[24] [see Fig. 1(a) and Fig. S1 of the supplementary material].

B. Adiabatic potentials and coupling terms

By dipole selection rules for the $D_{\infty h}$ symmetry of N_2, single-photon VUV excitation couples the ground $^1\Sigma_g$ state of N_2 only to $^1\Pi_u$ and $^1\Sigma_u$ excited states. We assume the molecules are aligned in the perpendicular direction to the laser pulse so that states of Π_u symmetry are excited exclusively. Strong nonadiabatic coupling is allowed only between the states of the same symmetry. Selection rules for the singlet-triplet interaction are as follows. Spin-orbit $l_z s_z$ component couples Π_u singlet and triplets states, while $l_x s_x / l_y s_y$ components can couple Π_u states to Σ_u or Δ_u states. Considering the energy range of interest, 100 000–112 000 cm^{-1}, we neglect the coupling of Π_u states to the singlet and triplet Σ_u and Δ_u states as they are lying lower/higher in energy.

Potentials and nonadiabatic couplings for the $^1\Pi_u$ and $^3\Pi_u$ states of N_2 in the frequency range of 90 000–130 000 are presented in Fig. 1. We use the label S for the singlets and T for the triplets. Both are of Π_u symmetry. We found strong coupling between the adiabatic singlet excited states to be largely localized in the Franck-Condon region [Fig. 1(a)]. The curvature of the potentials at longer interatomic separations reflects the different bonding nature of the states: the lowest singlet diabatic state has shallower anharmonic potential. S_2 and S_3 potentials follow closely the nearly harmonic diabatic curves of the Rydberg states and become coupled to higher lying repulsive states only in the energy range higher than 115 000 cm^{-1}. In the present work, we limit pulse excitation energies to the frequencies 100 000–112 000 cm^{-1}, where the effect of the higher states is negligible.

Adiabatic potentials of the triplet states have a more complicated shape [Fig. 1(b)] as one can observe at least 4 repulsive avoided crossings. Sketched as black dashed lines in Fig. 1(b) are smoothly interpolating diabatic potentials. The lowest repulsive state corresponds to the pathway toward the lowest in energy, N(^{4}S) + N(^{2}D) dissociation channel. The T_1-T_2 nonadiabatic coupling is the last stage before the final exit [see Fig. 1(c)]. The next repulsive state converges to the N(^{4}S) + N(^{2}P) dissociation channel, while the two highest repulsive terms correspond to the N(^{2}D) + N(^{2}D) channel.

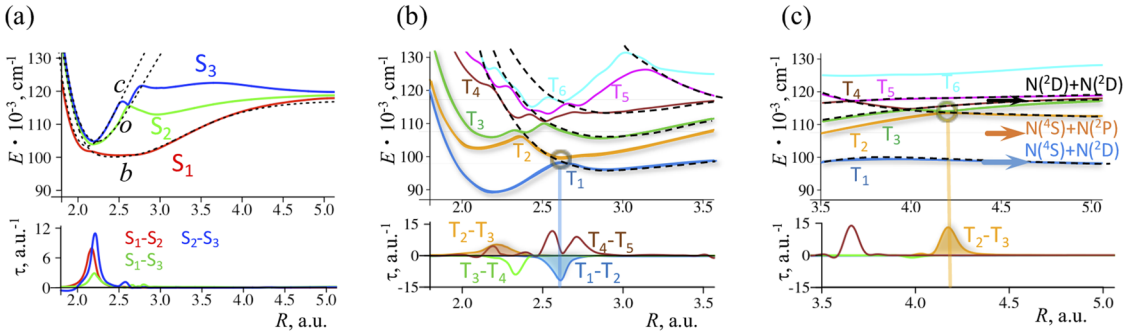

FIG. 1. Potentials and nonadiabatic couplings τ for the singlet (a) and triplet [(b) and (c)] states of N_2. Diabatic potentials for singlet states (*o*, *c*, and *b*) from the recommended set of Spelsberg and Meyer[24] are shown as black dashed lines on panel (a) for comparison. Nonadiabatic couplings between the triplet states are shown separately for the short (b) and long (c) range of interatomic distances. Strong coupling between T_1 and T_2 at short range and T_2 and T_3 at long range is highlighted. These couplings are the latest toward the two lowest, N(^{4}S) + N(^{2}D) and N(^{4}S) + N(^{2}P), dissociation channels. The complex shaped avoided crossings of the adiabatic triplet potentials can be described as crossing between the bound states and 4 dissociative diabatic terms (sketched as black dashed lines).

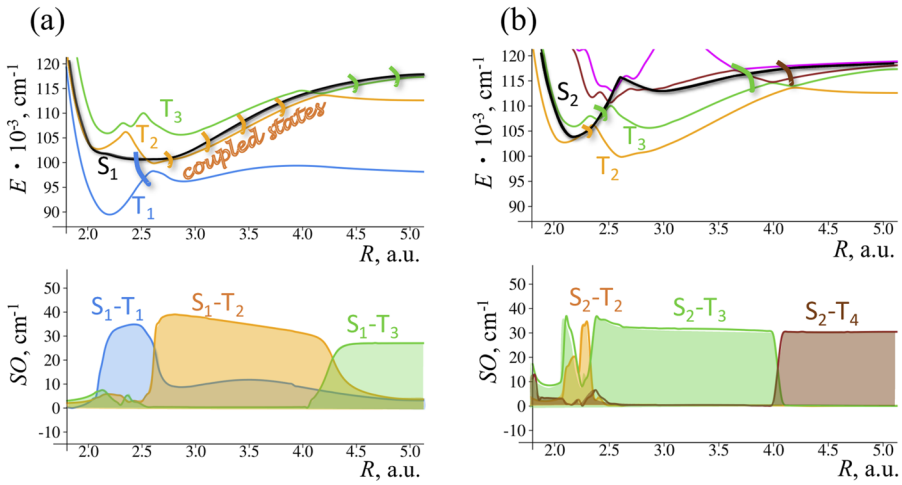

FIG. 2. Potentials and spin-orbit (SO) couplings for the adiabatic singlet S_1 (a), S_2 (b), and triplet states [(a) and (b): T_1—blue, T_2—orange, and T_3—green]. The regions of strong effective SO coupling between the singlet and different triplet states are shown schematically as stitches of the same color as the, respectively, coupled triplet state.

Spin-orbit (SO) couplings for the two lowest singlet states are shown in Fig. 2. The first singlet state has a large magnitude (30–40 cm^{-1}) coupling to the outer well of the adiabatic T_2 and to the bound part of the T_1 potential. The strength of the coupling agrees well with previously published value of 39 cm^{-1} and with its being independent of distance in the diabatic representation.[25]

The potential energies of S_1 and T_2 run near and parallel around the outer wall of S_1. As the effective coupling is inversely proportional to the energy gap between the coupled states, the strong S_1-T_2 singlet-triplet interaction spans a wide range of distances [Fig. 2(a)]. The spin-orbit coupling of the Rydberg singlet state, S_2, has similar magnitude of about 35 cm^{-1}; however, the energy gap between the singlet and T_2/T_3 states is small only in the narrow region of short distances [Fig. 2(b)]. The same picture was also found for the S_3 Rydberg state—where the large magnitude of the effective coupling to T_2 and T_3 is confined to the region of short interatomic separations. Triplet states are strongly coupled at this range of distances which makes it harder to relate with the previously known values for the spin-orbit coupling between the diabatic states G and F, bound triplet analogs to the singlet Rydberg states. As reported,[25] the magnitude of the coupling between the diabatic singlet *o* state and triplet F state is ~37 cm^{-1} which is close to our values of the spin-orbit coupling of S_2 and S_3 and T_2 and T_3 in the short region of distances.

In what follows, we study dynamics of the coherent wave packet induced by pulses with frequencies lower than 112 000 cm^{-1}. The strong nonadiabatic coupling between the states means that the kinetic energy is rather nonlocal in the nuclear coordinates and is off-diagonal in the electronic indices.[42] To take advantage of the fitting to spectroscopically accurate measurements, we move to the diabatic representation. In what follows for the singlet states, we use the diabatic set established by Spelsberg and Meyer,[24] while for the triplet states, we diabatize only the two low-lying adiabatic triplet states as will be described in Subsection II C.

C. Diabatic representation

As one can see from the magnitude of the spin-orbit interaction (Fig. 2), significant values are found only for the S_1-T_1 and S_1-T_2 coupling. To simplify the diabatization procedure, we therefore consider only the two lowest adiabatic triplet states, which are coupled in the range of R values 2.5–3.5 a.u. We neglect the nonadiabatic coupling of T_2 to higher lying triplets.

We use the well-known correspondence between the nonadiabatic coupling terms and derivatives of the angle θ, which determines the adiabatic-to-diabatic transformation matrix for a two state problem[43,44]

$$\frac{\partial\theta_{12}}{\partial R} = \tau_{12}(R) = \left\langle \varphi_1 \middle| \frac{\partial\varphi_2}{\partial R} \right\rangle,$$
$$\frac{\partial^2\theta_{12}}{\partial R^2} = Y_{12}(R) = \left\langle \varphi_1 \middle| \frac{\partial^2\varphi_2}{\partial R^2} \right\rangle, \quad (1)$$

where $\tau(R)$ and $Y(R)$ are the first and second order nonadiabatic couplings, respectively. Knowing the nonadiabatic coupling terms defined on a grid of internuclear distances $\{R_n\}$ from the quantum-chemical computations, we can estimate the transformation angle at each grid point using the Taylor series

$$\theta_{12}(R_{n-1}) = \theta_{12}(R_n) - \left.\frac{\partial\theta_{12}}{\partial R}\right|_{R=R_n} \cdot a + \left.\frac{\partial^2\theta_{12}}{\partial R^2}\right|_{R=R_n} \cdot a^2 + O(a^3)$$
$$\approx \theta_{12}(R_n) - \tau_{12}(R_n) \cdot a + Y_{12}(R_n) \cdot a^2. \quad (2)$$

For small spacings a of the grid, this equation gives accurate approximation for the diabatic transformation matrix (we used a = 0.002 85 a.u.). We define the transformation in the region of 2.5–3.5 a.u. as the coupling between the triplet states is negligible outside of this range of interatomic separations. The value of the angle $\theta_{12}(R)$ for $R \geq 3.5$ a.u. was set to $\theta_{12}(R) = 0$.

Diabatic potentials and corresponding diabatic and spin-orbit couplings are shown in Fig. 3. Potentials and diabatic coupling V_{12} of the two triplet states are defined directly from the transformation angle at each grid point with the explicit results given in the supplementary material. To distinguish between adiabatic and diabatic potentials, we denote the long range repulsive diabatic triplet term as C′, while we denote the bound triplet state as C [Fig. 3(a)]. The resulted diabatic coupling between these triplet states is local-

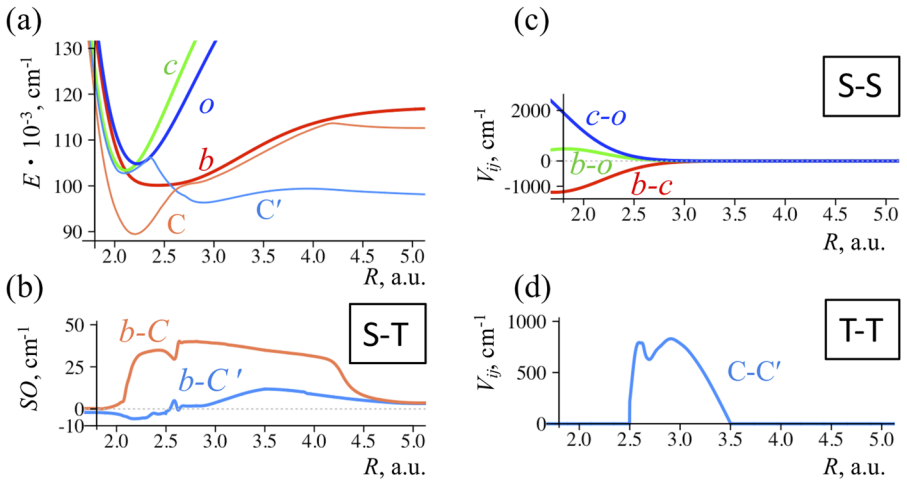

FIG. 3. Diabatic singlet and triplet potentials (a), spin-orbit, *SO*, (b), and diabatic couplings V_{ij} for the singlet (c) and triplet (d) manifold of states. For singlet states, valence *b*, Rydberg *o*, and *c* states, we used the recommended set of potentials and couplings of Spelsberg and Meyer.[24] Triplet states, bound *C*, dissociative *C*′, and their diabatic couplings were evaluated using the adiabatic-to-diabatic transformation matrix (as discussed in the text and the supplementary material).

ized in the region of crossing at $R \sim 2.5$–3.5 a.u. [Fig. 3(d)]. The spin-orbit couplings in the diabatic representation [Fig. 3(b)] were evaluated using a similar description of the triplet wave function in terms of adiabatic basis. We defined the SO-couplings only for the valence singlet diabatic state, neglecting the spin-orbit coupling for the Rydberg singlet states. This is justified for the low-frequency range of excitation energies as only the third diabatic triplet state is known to be coupled to the Rydberg *o* state.[25]

D. A model eigenstate basis

We define a basis set that diagonalizes all the terms in the electron-nuclear Hamiltonian apart from the weak spin-orbit coupling. The states of this basis are almost but not quite stationary. The diabatic coupling is diagonal so that the states have a mixed electronic character. But the singlet-triplet coupling remains off diagonal so that the states of the basis have a pure spin character. The states of the basis were determined by diagonalization[45] of the Hamiltonian matrix in the diabatic representation defined on a grid of the nuclear coordinate, *R*. We used 8-point finite difference formula for the definition of the kinetic energy operator on a grid.[46] Consequently, in the propagation of the wave function as a linear combination of basis states, there are two coupling terms. These are the spin-orbit and, at early times, the dipole couplings to the pulse. These couplings are easy to evaluate starting from the composition of each vibronic state in the original diabatic basis on the grid and respective coupling terms.

Computed singlet vibronic levels exactly match the vibronic levels fitted in the work of Spelsberg and Meyer[24] to quantitatively reproduce the experimental absorption spectrum. A comparison between the positions of the computed eigenstates of the bound triplet C state with available experimental and theoretical data[25,26] for $^{14}N_2$ and $^{15}N_2$ is presented in Fig. 4. Outside the energy region of strong T_1-T_2 coupling (energies higher than 102 000 cm^{-1}), the computed levels of the bound C state are in very good agreement with the results of coupled channel model[25,26] that were adjusted to reproduce experimental data.

Strong diabatic coupling mixes the bound C and repulsive C′ states; therefore, the manifold of triplet states has bound states embedded in a continuum. Diagonalization results in a band of states formed in the vicinity of each zero-order bound state level. Each band spans up to 200 cm^{-1} and consists of states with different amount of the bound state, as seen in Fig. 4. We check the convergence of the bands by adding more and more continuum states until the shape of the band is stabilized. The exit to the continuum requires the spin-orbit coupling of the singlet states to these bands of triplets. As we will discuss in the following, because the coupling is weak, the effectively coupled states need to be nearly resonant in energy. Compared to the singlets, the levels of the triplets are more sensitive to the mass as seen from panels Figs. 4(a) and 4(c)

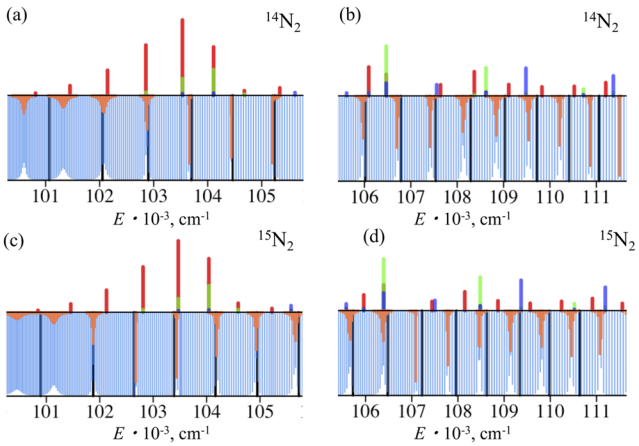

FIG. 4. Singlet (above the abscissa) and triplet (mirrored below the abscissa) vibronic energy levels shown vs their energy for $^{14}N_2$ [(a) and (b)] and $^{15}N_2$ [(c) and (d)], calculated for the model eigenstate basis. The possibly mixed character of each vibronic state is indicated by the colors. The stick heights of the optically active singlet levels are computed as the absolute value squared of the transition dipole moment multiplied by the weight of the valence *b*, Rydberg *c*, and *o* states (red, green, and blue sticks, respectively) in each vibronic state. Triplet vibronic levels are shown in the mirror panel with the height of each stick defined as the weight of the C′/C (blue/orange sticks) diabatic states in the composition of the vibronic level. Triplet levels of the pure C state calculated by Lewis *et al.*[25,26] are shown in black lines. The energies are given relative to $v = 0$ of the ground state.

or Figs. 4(b) and 4(d). This modulates the overall isotope effect in the dissociation.

III. QUANTUM DYNAMICS

A. Details of the field-induced quantum dynamics computations on a grid

We model the isotope effect on the dissociation yield by solving the dynamics in the manifold of four singlets: ground state, valence b, Rydberg c, and o states and two triplets: C′ and C coupled electronic states on a grid of nuclear coordinate. Coefficients of the basis functions at each grid point are propagated using the fourth order Runge-Kutta method[47] for the time-dependent Schrödinger equation

$$i\hbar\frac{dc_{kg}(t)}{dt} = \left(E_{kg} - iE_g^{CAP}\right)c_{kg} - \frac{1}{2m}\left(T_0 c_{kg} + \sum_{n=1}^{4} T_n\left(c_{kg-n} + c_{kg+n}\right)\right) + \sum_{j\neq k}\left(V_g^{kj} - \varepsilon(t)\mu_g^{kj}\right)c_{jg} + i\sum_{j\neq k} SO_g^{kj} c_{jg}. \quad (3)$$

The terms in the first line are diagonal in the electronic index k and consist of diabatic potential at the current grid point, $E_{kg} = E_k(R_g)$, complex absorbing potential (CAP), $E_g^{CAP} = 0.01 \cdot (R_g - 6.5)^3\,\Theta(R_g - 6.5)$, and kinetic energy terms. The unit Heaviside step function $\Theta(x)$ limits the complex-absorbing potential to act only in the region $R > 6.5$ a.u. This potential is used to accumulate population in the far dissociation region in all electronic states. Local and nonlocal kinetic energy terms, T_0 and T_n, are defined according to a finite difference approximation scheme of the second derivative.[48] For computations of the dynamics in different isotopomers, we use a different reduced mass m. We use an 8th order[46] scheme and a rather small grid spacing ($a = 0.002\,85$ a.u.) to simulate quantum dynamics accurately on a longer time scale.

Off-diagonal terms in the electronic index are responsible for the population transfer between the electronic states. The diabatic, V_g^{kj}, and spin-orbit, SO_g^{kj}, couplings were discussed in Sec. II C, Fig. 3. The ultrafast field couples the ground state to the excited electronic states and is represented explicitly as a time-dependent part of the Hamiltonian $\varepsilon(t)\mu_g^{kj}$, where μ_g^{kj} are transition dipole moments between the field-free electronic states $|\varphi_k(R_g)\rangle$ and $|\varphi_j(R_g)\rangle$. The profile of the field is characterized by the Gaussian envelope and optical carrier

$$\varepsilon(t) = \boldsymbol{\varepsilon}_p \exp\left(-(t-t_p)^2/2\sigma^2\right)\left[\cos(\omega t + \varphi) - \frac{(t-t_p)}{\omega\sigma^2}\sin(\omega t + \varphi)\right]. \quad (4)$$

The second term in the carrier field is needed to insure that the integral over the entire time-range of the pulse is zero $\int E(t)dt = 0$. The parameters of the envelope—the mean value t_p and the variance σ—define the excitation time and duration of the pulse, while the frequency ω and carrier-envelope phase φ determine the shape of the profile. The polarization direction of the field and its maximum amplitude is defined by the vector $\boldsymbol{\varepsilon}_p$. The frequency of the pulses was set to be resonant either with the low energy ($\omega = 102\,800$ cm^{-1}) or high-energy ($\omega = 108\,500$ cm^{-1}) part of the absorption spectrum. The tail to tail duration of the low-energy pulse was set to 19.2 fs ($\sigma = 3.2$ fs), corresponding to the 5000 cm^{-1} width of the pulse in the energy domain. This frequency range covers at least 7 lowest singlet vibronic states with mainly valence electronic character [Figs. 4(a) and 4(c)]. The high-energy pulse was chosen to be wider in frequency—8000 cm^{-1}, a 12 fs pulse ($\sigma = 2$ fs)—to excite more vibronic states in the coherent wave packet. In this energy range, there are states of pure valence and Rydberg, as well as mixed valence-Rydberg character [Figs. 4(b) and 4(d)]. The maximum amplitude $|\boldsymbol{\varepsilon}_p|$ for both pulses was set to 7×10^{-4} a.u., which corresponds to an intensity of 3.43×10^{10} W/cm^2.

B. Details of the quantum dynamics computations in the model eigenstate basis

We also report results for which the wave function is propagated in the basis of model eigenstates $|e_k\rangle$ (see Sec. II D) to clarify the mechanism of the isotope selectivity. This is because we expect that resonance conditions between singlet and triplet eigenstates that have a narrow range in energy, see Fig. 4, have a dominant role. Technically, we write the wave function as

$$\Psi(t) = \sum_k C_k(t)|e_k\rangle. \quad (5)$$

The coefficients C_k of each singlet or triplet state $|e_k\rangle$ in the expansion are calculated using the fourth order Runge-Kutta method[47] for the time-dependent Schrödinger equation

$$i\hbar\frac{dC_k(t)}{dt} = E_k C_k - \varepsilon(t)\sum_{j\neq k}\mu_{kj}C_j + i\sum_{j\neq k} SO_{kj}C_j. \quad (6)$$

Here, E_k are the energies of the state $|e_k\rangle$, while μ_{kj} and SO_{kj} are the dipole and the spin-orbit coupling matrix elements between a pair of eigenstates $|e_k\rangle$ and $|e_j\rangle$, respectively. The ultrafast pulse represented explicitly by the profile of the time-dependent field, $\varepsilon(t)$, is acting at the early times of the dynamics. After the field is over, the population of the eigenstates is changing only due to the weak spin-orbit interaction; therefore, one can trace particular states that contribute most to the overall singlet-triplet transfer.

IV. RESULTS AND DISCUSSION

A. Dynamics en route to dissociation

In the course of the short excitation pulse, it is the singlet states that are directly excited. The weak singlet-triplet coupling takes time to transfer population to the triplet manifold. After the pulse, there is about a 100 fold excess of population in the singlets; see Figs. S2 and S3 of the supplementary material. This slow leakage of population from the bound singlet manifold is the bottleneck in the unimolecularlike dissociation. There is however an additional feature. Past the bottleneck, the molecule is not yet in the continuum. The coupling of the singlets is to the bound triplet, and it is the strong diabatic coupling between the bound and dissociative triplet states that leads to the exit.

Following the pulse, there is an extensive dynamics in the singlet manifold; see Fig. 5 and also Fig. S4 in the supplementary material. The strong diabatic coupling mixes the valence and Rydberg states and gives rise to a strong isotope effect in the transfer.[18]

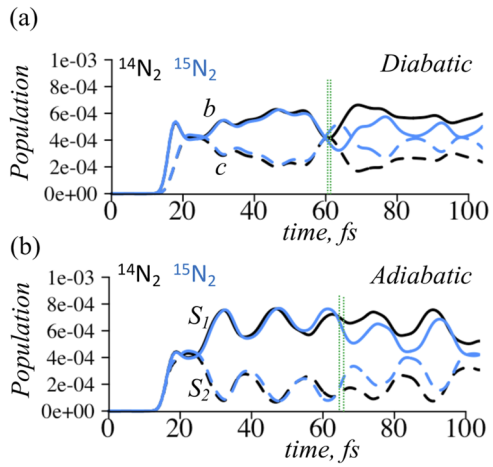

FIG. 5. Isotope effect in the population dynamics of singlets in diabatic (a) and adiabatic (b) representation for the two-state case using the higher energy pulse. Shown in the diabatic basis are the populations of the valence *b* [(a), solid lines] and Rydberg *c* [(a), dashed lines)] states. In the corresponding adiabatic picture shown are the populations in the states S_1 [(b), solid lines)] and S_2 [(b), dashed lines]. The plots also show that in either basis, there is extensive state mixing. The vertical dashed green lines indicate the beginning of the strong isotope effect. The isotope effect for the realistic three state coupling is shown in Fig. S2 of the supplementary material.

As seen in Fig. 5, there is also strong population transfer between the adiabatic states that is similarly accompanied by an isotopic differentiation. In either basis, the isotope effect is delayed until the vibrational wave packets on different electronic states come into overlap. This gives rise to a constructive interference in the population transfer as previously discussed.[18] The overlap of nuclear wave packets around 60 fs is imprinted on the dynamics in the singlet manifold (see movies S1–S4 in the supplementary material). The weak and continuous coupling to the triplets acts as a probe of the essentially unperturbed singlet dynamics. Thereby, the isotope effect survives for a long time of the dynamics (see Fig. S2 of the supplementary material).

When one analyzes the singlet triplet transfer in the model eigenstate basis, one can discern two quite different modes of behavior. One is when the states are nearly resonant in energy, and the transfer is efficient. Resonant here means energies well within the narrow window, ±40 cm^{-1}, of spin-orbit coupling. Otherwise, the population oscillates on a short time scale in the manner of Rabi oscillations.[49] These oscillations are also seen in the grid computations [using Eq. (3)] where dissociation is explicitly possible; see Fig. 6 and Fig. S5. The dynamics in the basis of eigenstates [Eq. (6)], see movies S5–S8 in the supplementary material, supports that the efficient transfer occurs through the levels that are resonant. The low frequency oscillations seen in Fig. 6 can be directly attributed to coherent oscillations in the populations of quasiresonant singlet and triplet eigenstates.

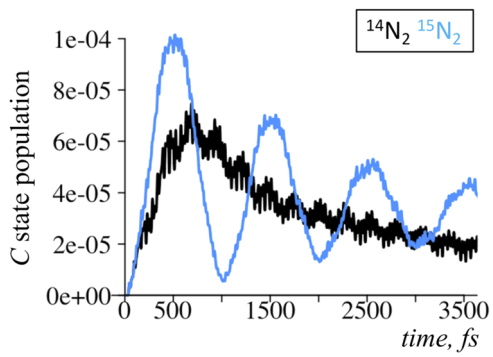

FIG. 6. Population dynamics in the bound triplet state C that is directly coupled to the singlet valence state b. Computed on a grid of nuclear coordinate for the two isotopomers as identified by the color, for the case of the lower energy pulse using Eq. (3). This figure shows the probing of the singlet manifold by the triplet state. The very fast oscillations, about 50 fs, are the period of the vibration of the valence singlet state. The lower frequencies reflect the mass-dependent resonance conditions. In $^{14}N_2$, the states are either well matched in energy or are further apart, 127 cm^{-1}, resulting in high oscillations of 262 fs. In $^{15}N_2$, the states are quasiresonant with Rabi oscillations at a higher period of about 1 ps (see also movies S5 and S6 in the supplementary material).

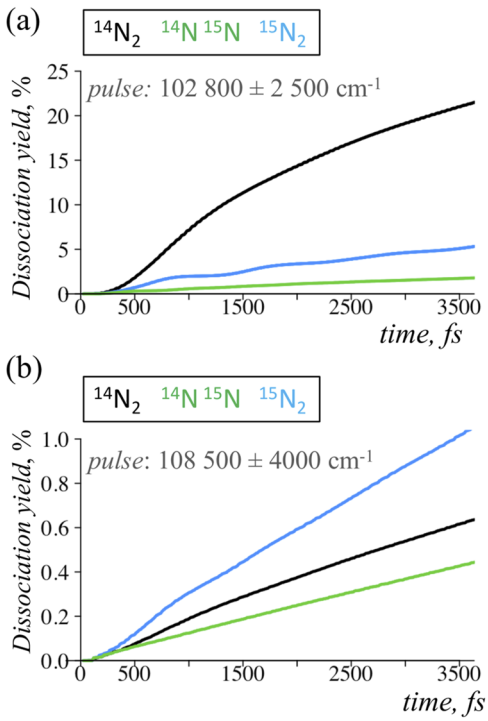

FIG. 7. Isotope effect in the photodissociation yield for $^{14}N_2$ (black line), $^{14}N^{15}N$ (green line), and $^{15}N_2$ (blue line). Computations on a grid of nuclear coordinates with a complex absorbing potential to account for the dissociation. The yield is given relative to the total population of the singlet excited states in per cents and differs to a large extent for the two pulses. The effect of mass is inverted for the two pulses studied. (a)—low-energy pulse (the mean frequency and width is noted in gray), (b)—higher energy pulse for which the singlet states are more mixed and have a lower valence state character, compare the panels on the left and the right in Fig. 4. Also, in the higher energy range, the resonance conditions are not as well satisfied.

The resonance condition of vibronic levels is mass dependent because the vibrational levels are. The mass shift is larger in the triplets, which have a higher vibrational quantum number, than for the singlets. The shift is typically larger than the width of the singlet-triplet resonance condition; see Fig. 4. The isotope effect of the resonances modulates the effect generated in the singlets and leads to the energy and mass dependent yield of dissociation.

B. Isotope effect in the yield of dissociation

The strong isotope effect and its energy dependence can be seen in Fig. 7. For the low energy pulse, the dissociation yield is about five-fold higher for $^{14}N_2$ compared to $^{15}N_2$. At the energy about the peak of the low energy pulse, the valence singlet state in $^{14}N_2$ is strongly resonant with the band of triplet states [Fig. 4(a)]. This is unlike the coupling for $^{15}N_2$. This difference is seen in Fig. 8(a), and it is consistent with the experimental predissociation linewidth[25] and with the theoretical predictions of the coupled channel model. The exception is the region around 101 500 cm^{-1}, about the crossing of the diabatic C/C′ states, where both states of both isotopomers have a low width. But unlike Ref. 25, we do not compute that $^{15}N_2$ is more strongly coupled to the triplet manifold. At a somewhat higher energy, about 103 500 cm^{-1}, there is a valence singlet state of $^{15}N_2$ that is effectively resonant [Figs. 4(c) and 8]. It is however coupled to a triplet adiabatic state that is largely bound, so the predissociation linewidth of this higher energy state of $^{15}N_2$ is also low. The dissociation yield of the mixed isotope $^{14}N^{15}N$ is somewhat lower because the coupling is to an adiabatic state that is even more bound in character. This shift of character arises because the energies of the triplet states shift more than the singlets upon isotopic substitution, as seen in Fig. 4.

Turning next to the higher energy pulse, the primary reason for the lower yield of dissociation is the narrower bottleneck to the triplets. This is because it is the valence singlet state that is primarily coupled to the triplets, and at the higher energy range, the singlet states are of much more mixed character [Figs. 4(b) and 4(d)]. Additionally, there are more effective resonances to states of $^{15}N_2$; therefore, there is a reversal of the sign of the isotope effect.

The recent experiments of Chakraborty *et al.*[32] probe the isotope effect in the photodissociation of N_2 over a broad frequency range. A strong excitation energy dependence was observed, but invariably ^{15}N was preferentially produced. These experiments are not directly comparable because they used an incoherent broad excitation pulse. More work is needed to see if we can reproduce the reported trends in the energy dependence of the isotope effect in the dissociation.

Next, we examine in more detail the dynamics and the yield for the low energy pulse where the isotope effect is more dramatic [Fig. 7(a)]. Two aspects need comment, the high yield of dissociation and the large isotope effect. For the long term dynamics, the eigenstate picture is more intuitive. An instantaneous picture of the population composition in singlet and triplet eigenstates computed for the low energy exciting pulse 800 fs after excitation is shown in Fig. 8 for $^{15}N_2$ and $^{14}N_2$. Each stick is placed at the energy of the particular eigenstate. The composition of each eigenstate is the sum of the heights of sticks each representing the contribution of a particular diabatic state. For example, in Fig. 8(a), the wave packet pumped to the singlet manifold of $^{14}N_2$ consists of five eigenstates. The lowest three are pure valence states, and the higher two are a mix of valence and one Rydberg state. The respective wave packet for $^{14}N_2$ in the triplet manifold is represented in Fig. 8(c). The largely resonant triplet state has a 30/70 composition of bound and repulsive

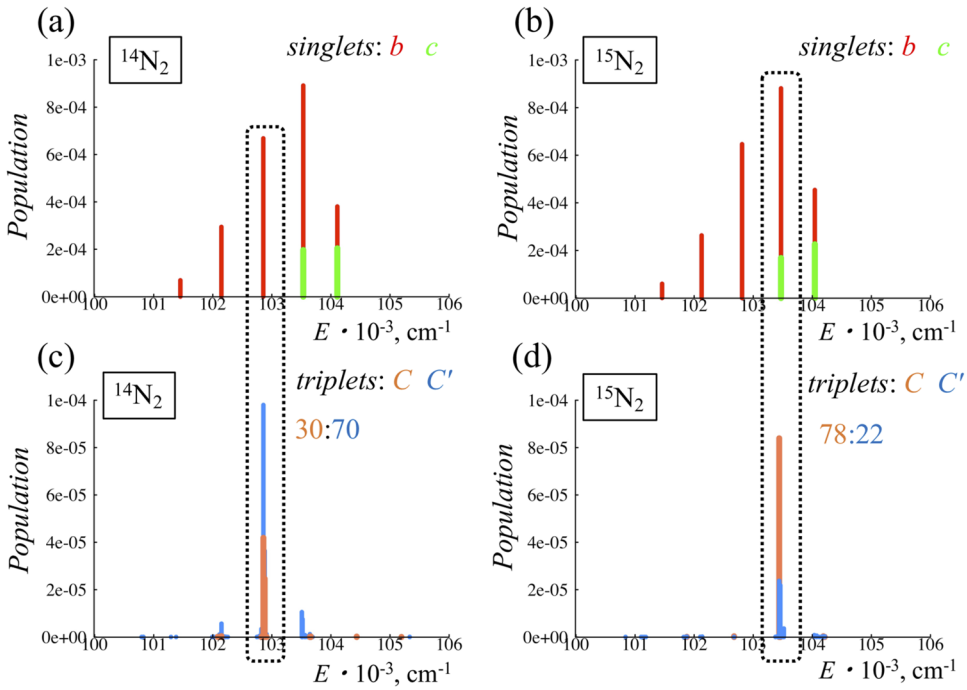

FIG. 8. Populations of wave packets in the singlet [(a) and (b)] and triplet [(c) and (d)] manifolds at 800 fs after excitation with the lower energy pulse. Left panels: the $^{14}N_2$ isotopomer. Right panels: $^{15}N_2$. The positions of the sticks are the energies of the model basis eigenstates where the ground state is at the zero of energy. In both the top and the bottom panels, for each position, we plot two sticks where the height of each stick is the population of the diabatic state, color coded as indicated in the inset.

diabatic triplet states. This is in contrast to Fig. 8(d) ($^{15}N_2$) where the composition of the largely resonant triplet state is almost opposite in character, 78/22. This explains much larger dissociation yield in the case of $^{14}N_2$. For the two triplet states, the ratio of the bound and dissociative states is shown and is seen to be opposite in the two isotopomers, explaining the favorable dissociation rate in $^{14}N_2$ seen in Fig. 7(a). Each eigenstate is a linear combination of diabatic states. For the lower energy singlets, these are primarily the valence excited *b* state and the *c* Rydberg state. The other singlet Rydberg state contributes significantly only at higher energies. While the figure is representative, the triplets probe the pulsating wave packet on the singlets, so the height of the sticks do depend on time and a time-dependent version of this figure is shown as the movies S5 and S6 in the supplementary material.

V. CONCLUDING REMARKS

The ultrashort fs VUV pulse excites N_2 to a coherent wave packet of several coupled singlet bound electronic states. The energy span of this excited superposition of states exceeds the vibrational spacings of the states involved so that there is a motion of a nuclear wave packet on each electronic state. Our quantum dynamical simulations show that the singlet-triplet bottleneck for the exit of the coherent wave packet into the dissociative continuum is controlled by singlet-triplet resonance conditions. The spin-orbit coupling, 40 cm^{-1} at most, is much smaller than typical spacing between the singlet or triplet vibrational levels; therefore, effective spin orbit transfer is better described as a "level-to-level" picture. In the language of perturbation theory, one can say that to lowest order, the dynamics in the singlet manifold is unperturbed by the dissociation. Following the transfer, there is considerable nonadiabatic coupling in the triplet manifold en route to dissociation.

For an ultrafast excitation, the time history of the system is that there is a period where the molecule samples its bound singlet phase space. The fast motion is that of wave packets on each singlet electronic state. The electronic states are coupled and their population changes in time whether one uses an adiabatic or a diabatic basis. In the energy regime of strong mixing, the mass-dependent population transfer between the electronic states is seen in either basis for the electronic states; see Fig. 5.

The singlet-triplet interaction is weak, and so it can couple only a narrow band of triplet states in a window of the order of this coupling that is tenfold smaller than the spacing of the bound singlet vibronic states. This coupling populates those energy components of the coherent singlet manifold wave packet that are quasiresonant. Whether triplet states that energetically can be resonant are or are not available depends on the mass and on the energy range. The mass-dependent resonance and the subsequent nonadiabatic coupling in the triplet states can give rise to different dynamics in different isotopomers. The resulting isotopic differentiation can reach thousands of permilles.

SUPPLEMENTARY MATERIAL

Numerical data on our computed potential energy surfaces, nonadiabatic, and singlet-triplet couplings for adiabatic and diabatic states, composition of the adiabatic states as a function of internuclear separation, plots and movies for the dynamics of the singlet and the triplet populations in the grid, and model eigenstate basis are available in the supplementary material.

ACKNOWLEDGMENTS

This work was supported by the AMOS program within the Chemical Sciences, Geosciences and Biosciences Division of the Office of Basic Energy Sciences, Office of Science, U.S. Department of Energy, Award No. DE-SC0012628 and by the Horizon2020 FET Open Project No. COPAC 766563. F.R. acknowledges support from the Fonds National de la Recherche Scientifique, Belgium (F.R.S.-FNRS).

REFERENCES

[1] A. H. Zewail, *Femtochemistry: Ultrafast Dynamics of the Chemical Bond* (World Scientific, Singapore, 1994).
[2] A. H. Zewail and R. B. Bernstein, "Real-time laser femtochemistry viewing the transition from reagents to products," Chem. Eng. News **66**, 24 (1988).
[3] M. Nisoli, P. Decleva, F. Calegari, A. Palacios, and F. Martín, "Attosecond electron dynamics in molecules," Chem. Rev. **117**, 10760 (2017).
[4] J. S. Ajay, K. G. Komarova, S. Van Den Wildenberg, F. Remacle, and R. D. Levine, *Attosecond Molecular Dynamics* (The Royal Society of Chemistry, 2018), pp. 308–347.
[5] F. Remacle and R. D. Levine, "An electronic time scale in chemistry," Proc. Natl. Acad. Sci. U. S. A. **103**, 6793 (2006).
[6] B. Mignolet, R. D. Levine, and F. Remacle, "Localized electron dynamics in attosecond-pulse-excited molecular systems: Probing the time-dependent electron density by sudden photoionization," Phys. Rev. A **86**, 053429 (2012).
[7] M. F. Kling, C. Siedschlag, A. J. Verhoef, J. I. Khan, M. Schultze, T. Uphues, Y. Ni, M. Uiberacker, M. Drescher, F. Krausz, and M. J. J. Vrakking, "Control of electron localization in molecular dissociation," Science **312**, 246 (2006).
[8] W. Siu, F. Kelkensberg, G. Gademann, A. Rouzée, P. Johnsson, D. Dowek, M. Lucchini, F. Calegari, U. De Giovannini, A. Rubio, R. R. Lucchese, H. Kono, F. Lépine, and M. J. J. Vrakking, "Attosecond control of dissociative ionization of O_2 molecules," Phys. Rev. A **84**, 063412 (2011).
[9] A. Palacios, J. Feist, A. González-Castrillo, J. L. Sanz-Vicario, and F. Martín, "Autoionization of molecular hydrogen: Where do the fano lineshapes go?," ChemPhysChem **14**, 1456 (2013).
[10] M. Kübel, Z. Dube, A. Y. Naumov, D. M. Villeneuve, P. B. Corkum, and A. Staudte, "Spatiotemporal imaging of valence electron motion," Nat. Commun. **10**, 1042 (2019).
[11] F. Remacle, M. Nest, and R. D. Levine, "Laser steered ultrafast quantum dynamics of electrons in LiH," Phys. Rev. Lett. **99**, 183902 (2007).
[12] M. Nest, F. Remacle, and R. D. Levine, "Pump and probe ultrafast electron dynamics in LiH: A computational study," New J. Phys. **10**, 025019 (2008).
[13] M. F. Kling, P. von den Hoff, I. Znakovskaya, and R. de Vivie-Riedle, "(Sub-)femtosecond control of molecular reactions via tailoring the electric field of light," Phys. Chem. Chem. Phys. **15**, 9448 (2013).
[14] D. Keefer and R. de Vivie-Riedle, "Pathways to new applications for quantum control," Acc. Chem. Res. **51**, 2279 (2018).
[15] D. L. Bunker, *Theory of Elementary Gas Reaction Rates* (Pergamon Press, Oxford, 1966).
[16] M. Quack and J. Troe, "Specific rate constants of unimolecular processes. 2. Adiabatic channel model," Ber. Bunsengesellschaft Phys. Chem. **78**, 240 (1974).
[17] G. G. Hall and R. D. Levine, "Kinetics of unimolecular breakdown. I. Formal solution," J. Chem. Phys. **44**, 1567 (1966).
[18] J. S. Ajay, K. G. Komarova, F. Remacle, and R. D. Levine, "Time-dependent view of an isotope effect in electron-nuclear nonequilibrium dynamics with applications to N_2," Proc. Natl. Acad. Sci. U. S. A. **115**, 5890 (2018).
[19] G. Stark, B. R. Lewis, A. N. Heays, K. Yoshino, P. L. Smith, and K. Ito, "Oscillator strengths and line widths of dipole-allowed transitions in $^{14}N_2$ between 89.7 and 93.5 nm," J. Chem. Phys. **128**, 114302 (2008).

[20]J. P. Sprengers, W. Ubachs, and K. G. H. Baldwin, "Isotopic variation of experimental lifetimes for the lowest $^1\Pi_u$ states of N_2," J. Chem. Phys. **122**, 144301 (2005).
[21]J. P. Sprengers, W. Ubachs, K. G. H. Baldwin, B. R. Lewis, and W. U. L. Tchang-Brillet, "Extreme ultraviolet laser excitation of isotopic molecular nitrogen: The dipole-allowed spectrum of $^{15}N_2$ and $^{14}N^{15}N$," J. Chem. Phys. **119**, 3160 (2003).
[22]B. R. Lewis, S. T. Gibson, J. P. Sprengers, W. Ubachs, A. Johansson, and C. G. Wahlstrom, "Lifetime and predissociation yield of $^{14}N_2$ $b\ ^1\Pi_u$ ($v = 1$) revisited: Effects of rotation," J. Chem. Phys. **123**, 236101 (2005).
[23]A. N. Heays, R. Visser, R. Gredel, W. Ubachs, B. R. Lewis, S. T. Gibson, and E. F. van Dishoeck, "Isotope selective photodissociation of N_2 by the interstellar radiation field and cosmic rays," Astron. Astrophys. **562**, A61 (2014).
[24]D. Spelsberg and W. Meyer, "Dipole-allowed excited states of N_2: Potential energy curves, vibrational analysis, and absorption intensities," J. Chem. Phys. **115**, 6438 (2001).
[25]B. R. Lewis, S. T. Gibson, W. Zhang, H. Lefebvre-Brion, and J. M. Robbe, "Predissociation mechanism for the lowest $^1\Pi_u$ states of N_2," J. Chem. Phys. **122**, 144302 (2005).
[26]B. R. Lewis, A. N. Heays, S. T. Gibson, H. Lefebvre-Brion, and R. Lefebvre, "A coupled-channel model of the $^3\Pi_u$ states of N_2: Structure and interactions of the $3s\sigma_g F_3\ ^3\Pi_u$ and $3p\pi_u G_3\ ^3\Pi_u$ Rydberg states," J. Chem. Phys. **129**, 164306 (2008).
[27]D. A. Little and J. Tennyson, "An *ab initio* study of singlet and triplet Rydberg states of N_2," J. Phys. B: At., Mol. Opt. Phys. **46**, 145102 (2013).
[28]M. Hochlaf, H. Ndome, D. Hammoutene, and M. Vervloet, "Valence-Rydberg electronic states of N_2: Spectroscopy and spin-orbit couplings," J. Phys. B: At., Mol. Opt. Phys. **43**, 245101 (2010).
[29]Y. Song, H. Gao, Y. C. Chang, D. Hammoutene, H. Ndome, M. Hochlaf, W. M. Jackson, and C. Y. Ng, "Quantum-state dependence of product branching ratios in vacuum ultraviolet photodissociation of N_2," Astrophys. J. **819**, 23 (2016).
[30]E. R. Warrick, J. E. Baekhoj, W. Cao, A. P. Fidler, F. Jensen, L. B. Madsen, S. R. Leone, and D. M. Neumark, "Attosecond transient absorption spectroscopy of molecular nitrogen: Vibrational coherences in the $b'\ ^1\Sigma_u$ state," Chem. Phys. Lett. **683**, 408 (2017).
[31]S. O. Adamson, V. V. Kuverova, G. K. Ozerov, G. V. Golubkov, S. S. Nabiev, and M. G. Golubkov, "*Ab initio* calculation of the lowest singlet and triplet excited states of the N_2 molecule," Russ. J. Phys. Chem. B **12**, 620 (2018).
[32]S. Chakraborty, T. L. Jackson, B. Rude, M. Ahmed, and M. H. Thiemens, "Nitrogen isotopic fractionations in the low temperature (80 K) vacuum ultraviolet photodissociation of N_2," J. Chem. Phys. **145**, 114302 (2016).
[33]H. J. Werner and P. J. Knowles, "A second order multiconfiguration SCF procedure with optimum convergence," J. Chem. Phys. **82**, 5053 (1985).
[34]P. J. Knowles and H. J. Werner, "An efficient second-order MC SCF method for long configuration expansions," Chem. Phys. Lett. **115**, 259 (1985).
[35]D. A. Kreplin, P. J. Knowles, and H.-J. Werner, "Second-order MCSCF optimization revisited. I. Improved algorithms for fast and robust second-order CASSCF convergence," J. Chem. Phys. **150**, 194106 (2019).
[36]P. J. Knowles and H.-J. Werner, "An efficient method for the evaluation of coupling coefficients in configuration interaction calculations," Chem. Phys. Lett. **145**, 514 (1988).
[37]H. J. Werner, B. Follmeg, and M. H. Alexander, "Adiabatic and diabatic potential energy surfaces for collisions of CN($X\ ^2\Sigma^+$, $A\ ^2\Pi$) with He," J. Chem. Phys. **89**, 3139 (1988).
[38]H.-J. Werner, P. J. Knowles, G. Knizia, F. R. Manby, M. Schutz, P. Celani, W. Gyorffy, D. Kats, T. Korona, R. Lindh, A. Mitrushenkov, G. Rauhut, K. R. Shamasundar, T. B. Adler, R. D. Amos, A. Bernhardsson, A. Berning, D. L. Cooper, M. J. O. Deegan, A. J. Dobbyn, F. Eckert, E. Goll, C. Hampel, A. Hesselmann, G. Hetzer, T. Hrenar, G. Jansen, C. Koppl, Y. Liu, A. W. Lloyd, R. A. Mata, A. J. May, S. J. McNicholas, W. Meyer, M. E. Mura, A. Nicklass, D. P. O'Neill, P. Palmieri, D. Peng, K. Pfluger, R. Pitzer, M. Reiher, T. Shiozaki, H. Stoll, A. J. Stone, R. Tarroni, T. Thorsteinsson, and M. Wang, MOLPRO, version 2015.1, a package of *ab initio* programs, 2015, see http://www.molpro.net.
[39]T. H. Dunning, Jr., "Gaussian basis sets for use in correlated molecular calculations. I. The atoms boron through neon and hydrogen," J. Chem. Phys. **90**, 1007 (1989).
[40]R. A. Kendall, T. H. Dunning, Jr., and R. J. Harrison, "Electron affinities of the first-row atoms revisited. Systematic basis sets and wave functions," J. Chem. Phys. **96**, 6796 (1992).
[41]T. H. Dunning and P. J. Hay, in *Methods of Electronic Structure Theory*, edited by H. F. Schaefer (Springer US, Boston, MA, 1977), pp. 1–27.
[42]F. T. Smith, "Diabatic and adiabatic representations for atomic collision problems," Phys. Rev. **179**, 111 (1969).
[43]M. B. Faist and R. D. Levine, "Collisional ionization and elastic-scattering in alkali-halogen atom collisions," J. Chem. Phys. **64**, 2953 (1976).
[44]M. Baer, *Beyond Born-Oppenheimer: Electronic Nonadiabatic Coupling Terms and Conical Intersections* (Wiley, Hoboken, NJ, 2006).
[45]J. Rutter and F. Tisseur, DSYEVD LAPACK Driver Routine, University of Tennessee, University of California Berkeley, Univ. of Colorado Denver and NAG Ltd., 2016.
[46]B. Fornberg, "Generation of finite difference formulas on arbitrary spaced grids," Math. Comput. **51**, 699 (1988).
[47]W. H. Press, S. A. Teukolsky, W. T. Vetterling, and B. P. Flannery, *Numerical Recipes in Fortran 77: The Art of Scientific Computing*, 2nd ed. (Cambridge University Press, 1996).
[48]K. G. Komarova, F. Remacle, and R. D. Levine, "On the fly quantum dynamics of electronic and nuclear wave packets," Chem. Phys. Lett. **699**, 155 (2018).
[49]C. Cohen-Tannoudji, B. Diu, and F. Laloe, *Quantum Mechanics* (Wiley, New York, 1977), Vol. I, p. 413.